Draft version December 1, 2021
Typeset using LATEX twocolumn style in AASTeX631

Transit Hunt for Young and Maturing Exoplanets (THYME) VIII: a Pleiades-age association harboring a transiting planet from *Kepler* (NOW TWO TRANSITING SYSTEMS)

Madyson G. Barber,[1] Andrew W. Mann,[1] Benjamin M. Tofflemire,[2,*] Jonathan L. Bush,[1] Adam L. Kraus,[2] Daniel Krolikowski,[2] Andrew Vanderburg,[3] Matthew J. Fields,[1] Elisabeth R. Newton,[4] Dylan A. Owens,[1] and Mackenna L. Wood[1]

[1]*Department of Physics and Astronomy, The University of North Carolina at Chapel Hill, Chapel Hill, NC 27599, USA*
[2]*Department of Astronomy, The University of Texas at Austin, Austin, TX 78712, USA*
[3]*Department of Physics and Kavli Institute for Astrophysics and Space Research, Massachusetts Institute of Technology, Cambridge, MA 02139, USA*
[4]*Department of Physics and Astronomy, Dartmouth College, Hanover, NH 03755, USA*

ABSTRACT

We describe a young association (MELANGE-2) in the *Kepler* field with a known planet candidate (KOI-3876.01) with signs of youth. To better determine the age and membership of MELANGE-2, we combine archival light curves, velocities, astrometry, with new high-resolution spectra of stars nearby KOI-3866.01 spatially and kinematically. The resulting rotation sequence, lithium levels, and color-magnitude diagram of members are all an excellent match for the Pleiades, confirming the population is co-eval and providing an age estimate of 110±10 Myr. KOI-3876's observed properties are an excellent match to the group, confirming membership. MELANGE-2 may be part of the larger Theia 316 stream, also estimated to be ≃108 Myr. For KOI-3876, we revise the stellar and planetary parameters of the system, taking into account the newly-determined age. We fit the 4.5 yr light curve from *Kepler* and find that KOI-3876.01 is a $2.0 \pm 0.1 R_{\oplus}$ planet that orbits its star every 19.58 days on an eccentric ($e > 0.2$) orbit. KOI-3876 was previously flagged as a likely eclipsing binary, but we rule this out using radial velocities from APOGEE and statistically validate the signal as planetary in origin based on archival follow-up and its *Kepler* light curve. Given its overlap with the *Kepler* field, we expect MELANGE-2 to be valuable for studies of spot evolution on timescales of years and KOI-3876 to be a piece of the growing work on transiting planets in young stellar associations.

Keywords: exoplanets, exoplanet evolution, young star clusters- moving clusters, planets and satellites: individual (KOI3876)

1. INTRODUCTION

Stellar clusters and associations serve as critical benchmarks for stellar and planetary astrophysics. Stars in such groups formed from the same interstellar cloud, and hence share a common (or similar) age, abundance pattern, and initial space velocity. The common set of properties makes it significantly easier to assign properties to the whole population, providing age estimates that are more precise and accurate than general-purpose techniques used outside clusters (e.g., Gyrochronology; Barnes 2007; van Saders et al. 2016) and work on stars where ages are especially challenging (e.g., M dwarfs; Kiman et al. 2021). Such coeval associations are therefore, ideal for how studying how stellar and planetary properties evolve with time (Krumholz et al. 2019; Mann et al. 2016a).

Associations within the *Kepler* field have been especially valuable for stellar and planetary astrophysics. The ≃4.5 yr baseline and precise photometry enable precise measurements of rotation periods, even at older ages (e.g., Angus et al. 2015; Aigrain et al. 2015), providing some of the best constraints we have on the rotation evolution of stars past 1 Gyr (Meibom et al. 2011; Curtis et al. 2019). The four *Kepler* clusters (NGC 6866, NGC 6811, NGC 6819, and NGC 6791) have also provided

Corresponding author: Madyson G. Barber
madysonb@live.unc.edu

* 51 Pegasi b Fellow

a wealth of information about stellar mass-loss (Miglio et al. 2012), post-main-sequence stellar evolution (Corsaro et al. 2012), and the occurrence of planets inside clusters (Meibom et al. 2013).

The four known clusters in the *Kepler* field are all at distances of more than 1 kpc and ages $\gtrsim$500 Myr. While these older ages (compared to nearby young groups) fill an important niche in stellar spin down and post-main-sequence evolution, their distance from the Sun makes it challenging to study the low-mass members and search for small planets. The *K*2 mission covered many younger and more nearby clusters (Van Cleve et al. 2016; Rizzuto et al. 2017), but only for $\simeq$80 days at a time. Searching for long-period planets and studying longer-term spot evolution with *K*2 data was therefore only possible in regions that *K*2 covered by multiple campaigns (Rampalli et al. 2021). Additional young associations in the *Kepler* field would provide the invaluable $\simeq$4.5 yr baseline.

The availability of precise parallaxes and proper motions for millions of stars from *G*aia (Gaia Collaboration et al. 2016, 2021) has enabled the discovery of new coeval stellar associations (e.g., Meingast et al. 2019; Kerr et al. 2021). The `FriendFinder` code[1] (Tofflemire et al. 2021) was designed to take advantage of *G*aia data, by searching for potential co-moving 'friends' around a user-identified young stars. This method has already been useful in finding the 250 Myr MELANGE-1 association (Tofflemire et al. 2021) and age-dating a planet in the Musca region of Lower-Centarus-Crux (Mann et al. 2021).

With the goal of finding previously undiscovered associations with transiting planets, we ran `FriendFinder` on *Kepler* objects of interest suspected to be younger than Hyades based on their lithium levels in Berger et al. (2018). The most promising association was a group of stars nearby KOI-3876; the candidate members showed a color-magnitude diagram (CMD) consistent with the Pleiades (consistent with the lithium levels). Here we describe our work demonstrating that the population (MELANGE-2) is a co-eval 110 Myr group, $\simeq$300 pc from the Sun, and harbors two transiting planetary systems (KOI-3876 b and Kepler-970 b).

While the THYME survey was meant to focus on planets identified with *TESS*, KOI-3876 b was flagged as young by the same team and using the same methods as used extensively in the THYME and ZEIT series. Since the planet is not along the ecliptic, we opted to include it in the THYME survey series with a slight adjustment to the acronym.

The paper is organized as follows. In Section 2 we detail our initial selection of potential members of MELANGE-2. We list the range of archival and new data taken on candidate members of MELANGE-2 in Section 3. In Section 5 we demonstrate MELANGE-2 is a co-eval population and derive its overall properties and basic membership. Our effort to find known and new planets in MELANGE-2 is described in Section 4. We derive properties of the only identified planet in the association, KOI-3876 b, in Section 7, and statistically validate it in Section 7.1. We summarize our findings in Section 8 and briefly discuss the future utility of an association overlapping the *Kepler* field.

2. TARGET SELECTION

As part of our effort to identify known planets in previously undiscovered young associations we ran the `FriendFinder` code (Tofflemire et al. 2021) on all stars identified as young based on their lithium absorption (Berger et al. 2018); this initial seed list included KOI-3876. The `FriendFinder` algorithm uses *G*aia EDR3 positions, parallaxes, and proper motions to identify stars with similar Galactic tangential velocity and XYZ position to a selected input source. This required an absolute velocity for KOI-3876, for which we used the value from APOGEE (-26.79km s^{-1}, Jönsson et al. 2020).

The lithium levels suggested an age for KOI-3876 close to the Pleiades. Unbound or weakly bound associations >100 Myr should be significantly dispersed as they orbit through the Galaxy (this needs a citation). So we used a generous selection, including any star within 5km s^{-1} and 50 pc of KOI-3876 as a candidate member. This yielded 1007 candidates.

We show the color-magnitude diagram (CMD) for our candidate members in Figure 1. The spread of the CMD suggests significant contamination; it is likely that most of the 1007 stars selected are not associated with KOI-3876. However, the CMD also shows there is significant contamination, there is also a sequence of the closest stars (in tangential velocity) consistent with the Pleiades single-star sequence. This matches the age suggested by the Li levels in KOI-3876.

3. OBSERVATIONS

3.1. *Optical spectra from McDonald 2.7 m Coudé*

We observed KOI-3876 and 21 association candidates (Section 2) with the Coudé spectrograph on the Harlan J. Smith 2.7m telescope at the McDonald Observatory. The Robert G. Tull Coudé is a cross-dispersed echelle spectrograph, delivering a R$\sim$60,000 spectral resolution

[1] https://github.com/adamkraus/Comove

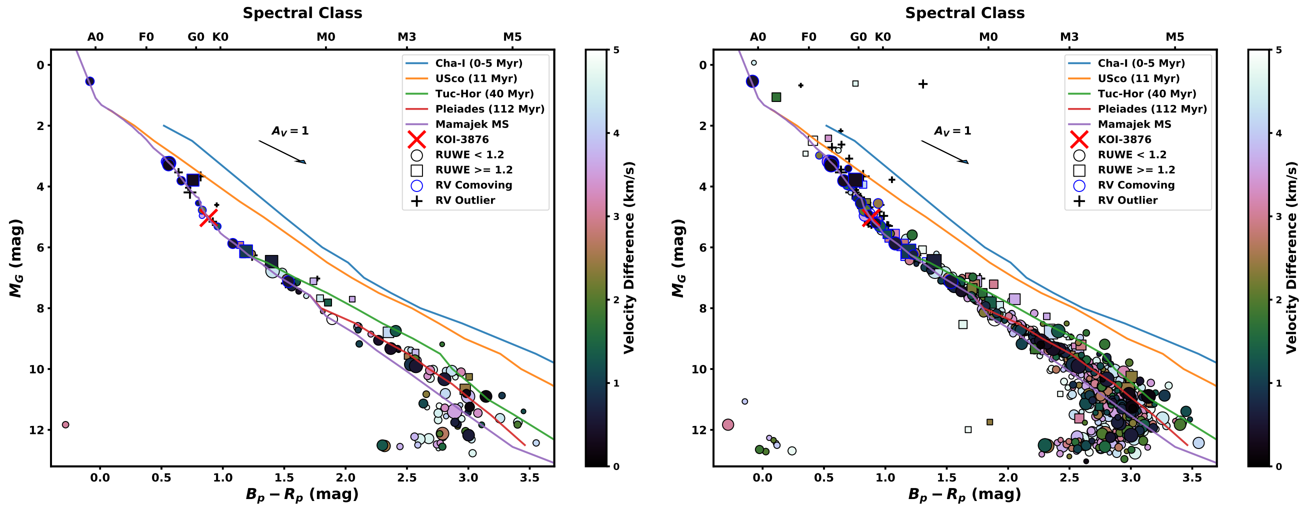

Figure 1. *G*aia color-magnitude diagram of all stars within 5 km s^{-1} in tangential velocity and 25 pc (left) or 50 pc (right) of KOI-3876. Approximate spectral types are shown on the top axis. Points are color-coded by the difference between their expected and observed tangential velocity assuming a perfect UVW match to KOI-3876 and scaled in size by their distance from KOI-3876. Points with radial velocities consistent with KOI-3876 are marked with blue circles and those with discrepant velocities are changed to a plus signs (and excluded from the color coding). Approximate single-star sequences from major nearby groups with known ages are shown as colored lines. These have not been corrected for reddening and are only used as a rough guide to the expected sequence.

from 3400–10000 Å using the 1.″2 slit (Tull et al. 1995). Observations we're taken over the course of two observing runs, on 2021 July 9 and 2021 August 26–27. The sample was selected to include association candidates that could be observed with the Coudé in modest exposure times ($G < 13$), and spectral types later than mid-F ($B_p - R_P > 0.55$), where we expect lithium absorption to be a sensitive age diagnostic. The spectra are reduced with a custom python implementation of the standard IRAF procedures. Wavelength calibration made use of ThAr lamp spectra taken at the beginning, middle, and end of each night. the signal-to-noise of our spectra ranged between 14 and 60 per resolution element.

To assess whether association candidates are co-moving in three dimensions, we measure radial velocities using spectral-line broadening functions (BFs). The BF is a linear inversion of an observed spectrum with a narrow-lined template, and represents the average stellar absorption-line profile. This profile (the BF) can be fit with a rotationally-broadened line profile to measure the stellar radial velocity and $v \sin i_*$. We compute BFs for 34 spectral orders between 4300 and 9800 Åthat are free of telluric contamination using the `saphires` python package (Tofflemire et al. 2019). BFs from individual orders are combined in to a single, high SNR BF and fit with a rotationally broadened profile (Gray 1992). Narrow-lined templates, specific to each star, are taken from the Husser et al. (2013) PHOENIX model suite at the $T_{\rm eff}$ closest to that provided by the *TESS* Input Catalog (v8.0; Stassun et al. 2019). Radial-velocity errors depend on the S/N and rotational broadening, but are generally on the order of 0.1 km s^{-1}. Measurements from the Coudé spectra are provided in Table 4.

3.2. *Kepler and TESS light curves*

3.2.1. *Light curves for transit search and characterization*

We searched for *Kepler* photometry for all 1007 candidates within the Mikulski Archive for Space Telescopes (MAST). A total of 84 targets had *Kepler* data, the majority of which had data from all quarters (Q0-Q17). We restricted our analysis to long-cadence data (30 m), as short-cadence was not available for any of the planet hosts. For those lacking *Kepler* data, we instead downloaded *TESS* photometry wherever it was available through MAST. This included 15 targets with 2-minute cadence data, and 41 targets with 30-minute cadence data from the Quick-Look Pipeline (QLP; **?**).

Where possible, we used the Pre-search Data Conditioning Simple Aperture Photometry (PDCSAP; Smith et al. 2012; Stumpe et al. 2012). This included KOI-3876, all *Kepler* candidate members, and the 15 targets with 2-minute cadence from *TESS*. For the remaining, we used the Quick-Look Pipeline light curves (Huang et al, 2020; https://arxiv.org/abs/2011.06459) for our planet search. Table 4 lists which stars have *Kepler* and/or *TESS* photometry that was used for our planet search. More details on our transit search can be found in Section 4.

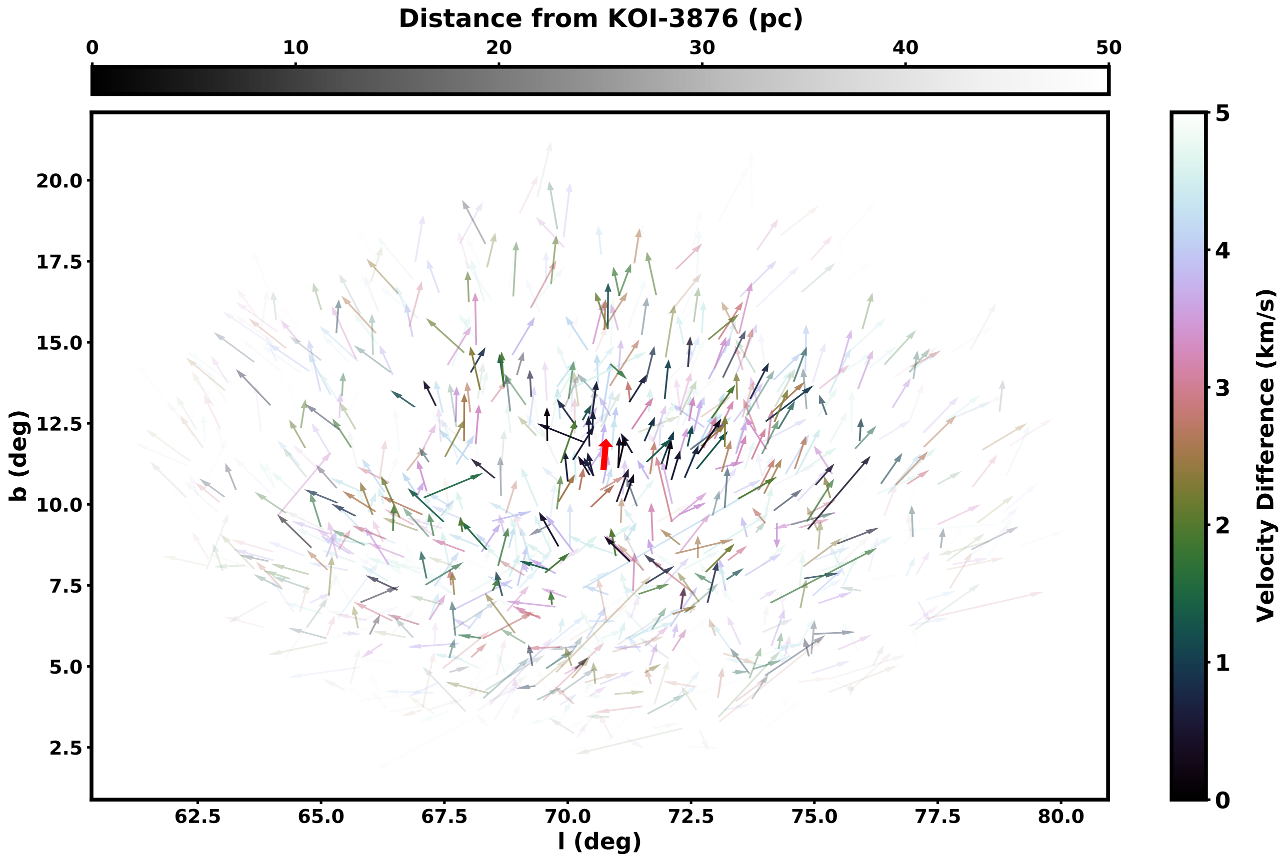

Figure 2. Galactic coordinates and motions for all 1007 candidate members of MELANGE-2. The red arrow shows KOI-3876, and other stars are color-coded by their tangential velocity offset from KOI-3876 with transparency set by their physical distance from KOI-3876. Arrows indicate the direction and (relative) magnitude of the proper motion.

The remaining 885 sources had no pre-extracted *TESS* or *Kepler* light curves. We did not extract additional curves from the full-frame *TESS* images for our planet search or characterization. The association association is more than 300 pc away; most of the remaining stars were too faint to extract a light curve precise enough for our planet search. However, many such systems are still useful for measuring rotation periods.

3.2.2. *Light curves and literature search for rotation*

To assess membership and age of MELANGE-2members, we collect stellar rotation periods using literature measurements supplemented by our own measurements from *Kepler* and *TESS* light curves. First, candidate members were cross matched against Nielsen et al. (2013), McQuillan et al. (2013, 2014), and Santos et al. (2019, 2021) for literature rotation periods. We matched candidate members to catalog members by *Kepler* Input Catalog (KIC) identifiers, which are listed in each catalog. We identified 56 candidate members with available literature rotations, all but five of which have rotation measurements in multiple catalogs. For candidates that appear in only one catalog, we adopt the single measurement value. In cases where a star had measurements from more than one source, we adopt the average of the measurements as the rotation period. Only one object, KIC 3743810, had a conflicting rotation periods between catalog sources. Based on a visual examination of this object's *Kepler* PDCSAP light curve we selected the value from Nielsen et al. (2013).

For stars without literature rotation periods we performed our own analysis. Priority was given to *Kepler* PDCSAP data followed by *TESS* full-frame images. To generate the *TESS* light curves for rotation analysis, we first created raw flux light curves from the FFI cutouts centered on each candidate. Then, we generated a Causal Pixel Model (CPM) of the telescope systematics using the `unpopular` package (Hattori et al. 2021) for each individual star. We subtracted the CPM systematics from the initial light curves, resulting in the light curves used for our rotation search described in Section 5.4.

3.3. *Archival photometry and astrometry*

We download positions, parallaxes, proper motions, and B_P, R_P and G photometry for all candidate members of MELANGE-2 using the third Gaia Early Data Release (EDR3; Gaia Collaboration et al. 2021). For KOI-3876, we also retrieved photometry from the Two-Micron All-Sky Survey (2MASS; Skrutskie et al. 2006), the Wide-field Infrared Survey Explorer (WISE; Cutri & et al. 2014), and the AAVSO All-Sky Photometric Survey (APASS; Henden et al. 2016). Photometry for KOI-3876 is listed in Table 2.

3.4. *Archival Velocities*

In order of preference, we drew radial velocities for candidate MELANGE-2 members from the second Gaia data release (DR2; Katz et al. 2019), the sixteenth APOGEE data release (DR16; Jönsson et al. 2020), and the fifth LAMOST data release (DR5; Luo et al. 2015, 2019). Velocities from our own spectra (Section 3.1) were given the highest priority. In the instance where a star had multiple velocities from the same star we used the weighted mean and error. We did not combine multiple velocities from different sources due to possible differences in the zero-points.

In total, we adopted Gaia RVs for 56 stars, APOGEE RVs for 5 stars, and LAMOST RVs for 25 stars. This was in addition to velocities from our Coude spectra for 22 candidate member stars as well as KOI-3876. We applied an offset to the LAMOST velocities of +4.54km s^{-1} based on the comparison from Anguiano et al. (2018). There may be additional zero-point differences between the velocity sources, but these are likely larger than the internal velocity spread within the group. The adopted velocities are given in Table 4.

4. SEARCH FOR PLANETS IN MELANGE-2

did you use notch and locor, or just notch? To check for other candidate planets or eclipsing binaries in the same association we searched the 265 *Kepler* and *TESS* light curves using the Notch pipeline pipelines. The details of both pipelines are described in more detail in Rizzuto et al. (2017). To briefly summarize, the Notch filter fits a window of the lightcurve as a combination of an outlier-robust second-order polynomial (for the stellar variability) and a trapezoidal notch (representing the potential planet). The window moves along the lightcurve until the variability is detrended while preserving the planet signal. At each data point, we calculate the improvement from adding the trapezoidal notch based on the change in the in Bayesian Information Criterion (BIC) compared to modelling just a polynomial. LOCoR (Locally Optimized Combination of Rotations), instead models the stellar variability using linear combinations of pseudo-rotation measurements in other parts of the light curve than the region being modeled. It then repeats this process over the full curve.

We searched the detrended light curves (both Notch and LOCoR detrended) and the BIC signals that Notch produces for periodic signals. We excluded the rotation period (and aliases) of the star, as it is common to have imperfect detrending with both algorithms. In addition to our search, a number of known *Kepler* objects of interest (KOIs) reside within candidate members of MELANGE-2, identified by a simple cross-match against the most recent KOI catalog (Twicken et al. 2016).

In total, we identified 18 targets of interest that are either KOIs and/or pass the SNR and initial quality checks from Notch/LOCor. Eight of these are known KOIs (KOI-678.01, KOI-678.02, KOI-966.01, KOI-966.02, KOI-1838.01, KOI-5304.01, KOI-6819.01, and KOI-7059.01), while the remaining are newly identified.

All 18 targets are listed in Table 1 along with our classification of each. Other than KOI-3876 b, we concluded only one other detection (Kepler-970 b) was both a real planet and a member of MELANGE-2. We discuss each system and our reasons for rejection them below.

4.1. *Discussion of individual candidates*

KOI-1838.01 is a confirmed planet (Kepler-970 b; Morton et al. 2016). The star's rotation (9.3 days) places it right on the Pleiades sequence, and much faster than the stalling regime seen for > 600 Myr systems (Curtis et al. 2019). The LAMOST (corrected) velocity is -32$\pm$4 km s^{-1}, which is consistent with the value predicted for membership ($\simeq$-27km s^{-1}). A more precise measurement from the CKS-cool project (Petigura et al. 2021) yielded an RV of -27.15$\pm$0.10km s^{-1}, a nearly perfect match for the association. The spectra shows weak lithium ($< 50 m\AA$), but this is consistent with 100 Myr for its spectral type CITE A MODEL. As we show in Figure 1, Figure 2, and Figure 5, Kepler-970 is consistent with MELANGE-2's color-magnitude diagram, proper motion, and Galactic position. ALL THREE PLOTS SHOULD BE UPDATED. We conclude that this planet is real and a member and include it in our analysis of KOI-3876.

KOI-678 (.01 and .02) contains two confirmed planets (Kepler-211 bc), and the star's light curve showed a clear rotation signature of $\simeq$13.7 days. However, this period is too long for membership given its Gaia colors (should be $\lesssim$8 days). Similarly, the lithium equivalent width is only 3.8$m\AA$ (Berger et al. 2018), but membership would suggest a Li level above 100$m\mathring{A}$. The star's proper motion also puts it on the outskirts of the distribution. We conclude this target is unlikely to be a member.

Both planet candidates in KOI-966 are flagged as false positives by the *Kepler* analysis (**?**), with both signals attributed to an eclipsing binary (.02 corresponding to an alias of the secondary eclipse). We similarly concluded that the signal is likely an eclipsing binary based on the V-shaped transit and secondary eclipse. The star's rotation period (3.92 days; Walkowicz & Basri 2013) is consistent with membership for an M dwarf and does not match the eclipse period (0.379 days). The star is also only 1km s^{-1} and 8 pc from KOI-3876, near the core of likely members. We conclude it is likely an eclipsing binary in the association.

KOI-6819 contains a planet candidate (.01). The star shows no significant rotation, suggesting the star is of older age. We find KOI-6819 has a radial velocity of 3.27km s^{-1} //gaia dr2//, >20km s^{-1} off from KOI-3876. KOI-6819 shows no Li signature, when we would expect >50$m\mathring{A}$. We conclude this target is unlikely to be a member.

KOI-7059.01 is flagged as a false positive by the *Kepler* analysis (**?**), and the odd-even depth difference strongly suggests and eclipsing binary. KOI-7059 is >48 pc from KOI-3876. We conclude this target is likely a real eclipsing binary but unlikely to be a member.

For the newly identified targets, KICs 1137886, 6134939, 6366739, 6589221, 9139566, and 9700914 and TICs 164461070, 20352534, 272486188, 273383615, 28768382, and 355909811, we ultimately find that the SNR is below what we required for significance. This was determined by the BIC score for each target, where we found the BIC was below our threshold of significance for all targets. Even targets with the most transit-like signal (U-shaped and of reasonable depth), such as KIC 6589221 shown in Figure 3 and KIC 9700914 shown in Figure 4, were deemed simply likely candidates.

TICs 28768382 and 272486188 and KICs 9139566 and 9700914 are unlikely to be members due to the >20km s^{-1} difference in expected versus actual radial velocity.

KIC 6589221, while is 42pc from KOI-3876, we find to be within 2.2km s^{-1} of KOI-3876 and have a radial velocity of -24.44km s^{-1} which is <2km s^{-1} from expected. The stellar rotation of ≃5.4 days closely matches the expected rotation period for its *G*aia color. Further, the star's proper motion closely matches KOI-3876. We conclude this target is likely to be a member.

KOI-1838.01, KOI-678.01, and KOI-678.02 are confirmed planets, while KOI-6819.01 is still considered a planetary candidate. Using existing spectra from Exofop (//cite//), radial velocities from Gaia (//cite//), and rotational periods and activity metrics where available, we conclude all KOIs except KOI-966 are likely not members of the association. Based on it's rotational period, KOI-966, a clear eclipsing binary, is still likely a member. Notch and LOCoR flagged KICs 1137886, 6134939, 6366739, 6589221, 9139566, and 9700914 and TICs 164461070, 20352534, 272486188, 273383615, 28768382, and 355909811 as interesting targets possibly containing one or more transiting bodies. Due to the low SNR, we just consider these candidates. We summarize all findings in Table 1.

Table 1. Planetary Candidates in MELANGE-2.

ID	Disposition	Probable Member?
KOI-678.01	Confirmed	N
KOI-678.02	Confirmed	N
KOI-966.01	EB	Y
KOI-966.02	EB	Y
KOI-1838.01	Confirmed	N
KOI-5304.01	FP	N
KOI-6819.01	Candidate	N
KOI-7059.01	EB	N
KIC 1137886	Candidate	
KIC 6134939	Candidate	
KIC 6366739	Candidate	
KIC 6589221	Candidate	Y
KIC 9139566	Candidate	N
KIC 9700914	Candidate	N
TIC 164461070	Candidate	
TIC 20352534	Candidate	
TIC 272486188	Candidate	N
TIC 273383615	Candidate	
TIC 28768382	Candidate	N
TIC 355909811	Candidate	

5. THE MELANGE-2 ASSOCIATION

5.1. *Position and Kinematics*

AWM: note to self, this needs some editing.

For each of the 1007 candidate members of MELANGE-2, we show show the Galactic XYZ position in Figure 5 and the proper motion in Galactic coordinates (l, b) in Figure 2. Since our initial search used a generous search of 50 pc and 5km s^{-1} (tangential) from KOI-3876,

We originally identified a group of 998 stars within 50pc and 5 km/s of KOI-3876using //friendfinder//.

As can be seen in Figure 5, most //give percentage// targets in the field have velocities greater than 4 km/s of KOI-3876, shown in pink. These are likely non-member background stars. However, we can see a cluster of high

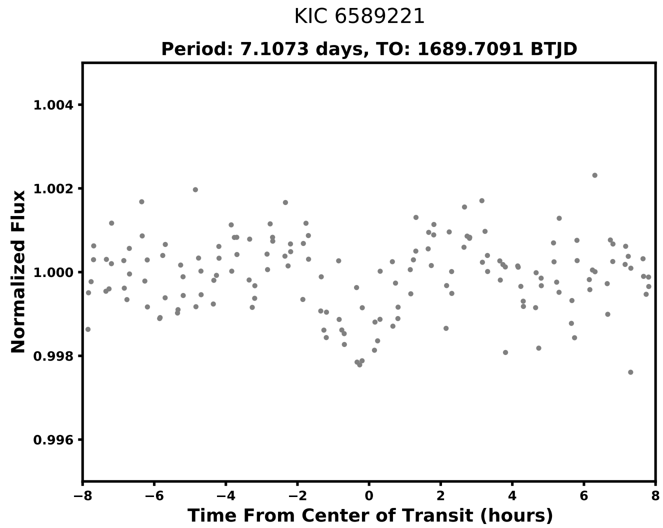

Figure 3. Phase-folded light curve of potential member KIC 6589221 from *TESS* detrended with Notch and LOCoR (grey points). We find that the bestfit period is 7.1073 days, with an initial transit time of 1689.709 BTJD.

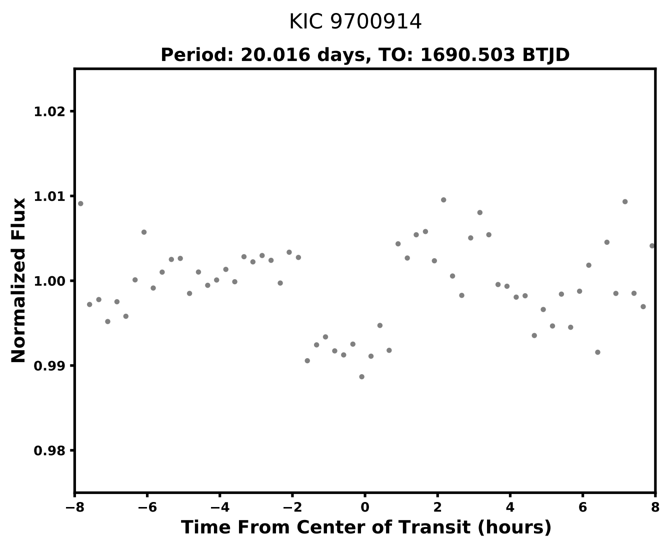

Figure 4. Phase-folded light curve of potential member KIC 9700914 from *TESS* detrended with Notch and LOCoR (grey points). We find that the bestfit period is 20.016 days, with an initial transit time of 1690.503 BTJD.

probability members that are within 1 km/s of KOI-3876, shown in black. We can see that these targets are tightly packed in z, between 58pc and 75pc, as expected based on the argument by //z argument paper//. In x and y, we see a streak as expected due to the rotation of the galaxy and the spreading of the cluster over time.

In Figure 2, we see a tight cluster of co-moving stars, shown in black surrounding KOI-3876, shown in red. We again see a large proportion of likely background stars moving separately from the core group.

5.2. *Isochronal age*

We estimated the age of MELANGE-2 by comparing the CMD to the PARSEC (v1.2S) models (Bressan et al. 2012). We used a mixture model, as detailed in Mann et al. (in prep)[2], based on the method outlined in Hogg et al. (2010), and wrapped in a Monte-Carlo Markov-Chain using `emcee` (Foreman-Mackey et al. 2013). To briefly summarize, we fit the population with the combination of two models. The first described the single-star member sequence drawn from PARSEC models. The second is an outlier population, which may itself contain a mix of populations (e.g., binaries, field interlopers, and stars with erroneous parallaxes or photometry). The fit included six free parameters: the association age (age), the average reddening across the association ($E(B-V)$), the amplitude of the outlier population (P_B), the offset of the outlier population from the main population CMD (Y_B [mags]), the variance of the outliers around the mean (V_B [mags]), and a term to capture missing uncertainties or differential reddening across the association (f [mags]).

Reddening was limited to < 0.2 mag based on the three-dimensional extinction map from Green et al. (2019). Other parameters evolved under uniform priors, bounded only by physical limits. We re-sampled the model grid to ensure uniform distribution around the expected age (50-250 Myr).

*G*aia photometry was the only available for all targets, and was generally far more precise than other data available. Many stars were also resolved as binaries (or the target and a background star) in *G*aia, but seen as a single source in 2MASS and KIC photometry (Brown et al. 2011). So we restricted our analysis to *G*aia magnitudes.

We expect most of the initial sample of 1007 candidate members to be field interlopers. While the mixture model can handle high contamination rates by making P_B larger, tests suggest the fit prefers call the true population of interest the outliers and instead fit the background population as the true one. To avoid this, we limited the input list to stars within 30 pc and 3km s^{-1} from KOI-3876 in three-dimensional distance and tangential velocity. We also removed any stars with a Renormalised Unit Weight Error (RUWE; Gaia Collaboration et al. 2021) > 1.2. As discussed in Ziegler et al. (2020) and Wood et al. (2021), stars above this limit are likely to be

[2] https://github.com/awmann/mixtureages

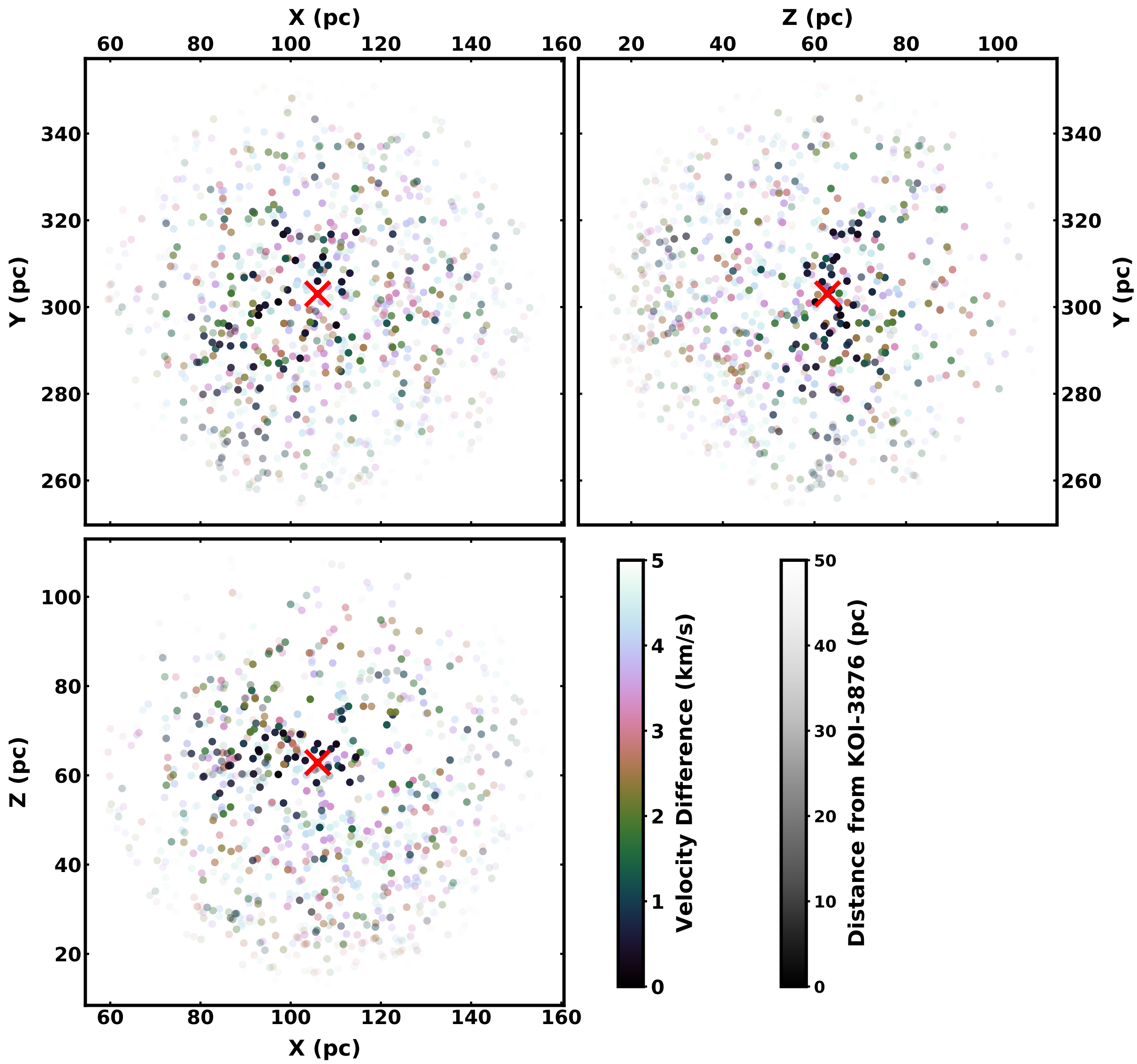

Figure 5. needs a caption here. Galactic Heliocentric (XYZ) coordinates of stars within 50pc and 5km/s of KOI-3876(marked as a red X). Color indicates the velocity difference from KOI-3876, and the transparency indicates distance from KOI-3876.

binaries. Lastly, we removed any stars that were outside the model grid range based on their absolute magnitude and/or color and stars with poor photometry or parallaxes (SNR<20). This left only 78 stars, but this was more than sufficient for a fit.

As we show in Figure 6, the resulting fit yielded an age of 104^{+8}_{-5} Myr. As a test of the systematic errors, we ran a similar fit using models from the Dartmouth Stellar Evolution Program (DSEP, Dotter et al. 2008) with magnetic enhancement described in Feiden & Chaboyer (2012). The DSEP-magnetic model fit gave a similar age of $110{\pm}11$ Myr. The DSEP magnetic models did somewhat better for the low-mass stars, and yielded a more conservative uncertainty, so we adopted this as the isochronal age.

5.3. *Lithium*

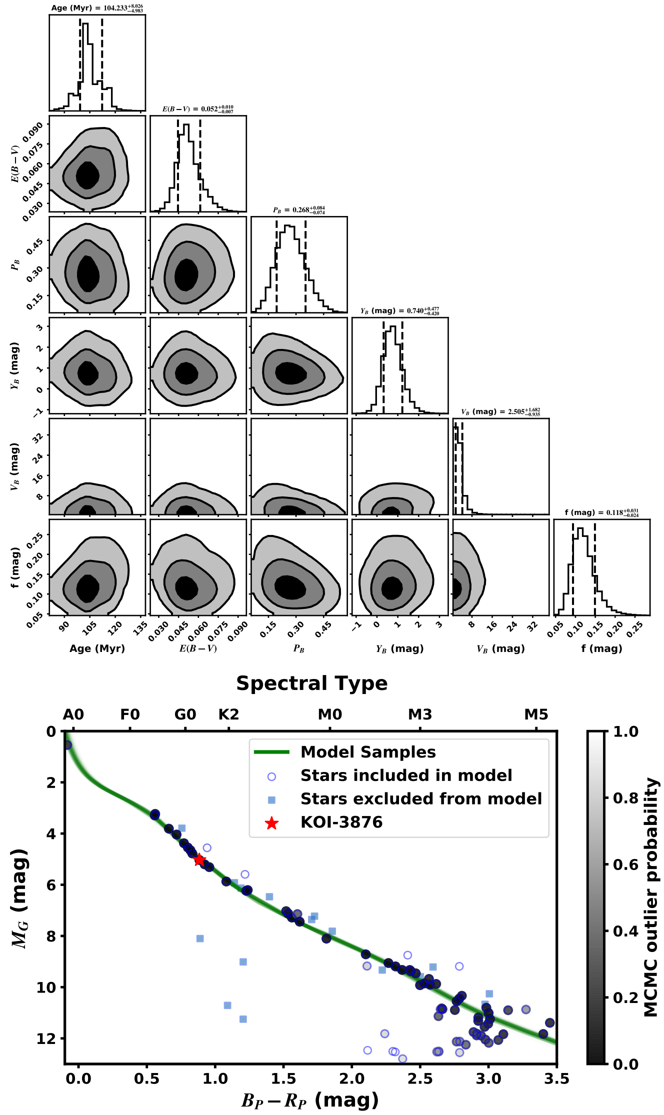

Figure 6. Comparison of the PARCSEC model isochrones to candidate members of MELANGE-2. The top shows the corner plot of our MCMC mixture model comparison, with contours corresponding to 1σ, 2σ, and 3σ. The bottom plot shows the Gaia G versus $G - R_P$ CMD of stars included in the MCMC (blue circles) and those excluded (blue squares) due to their RUWE, color, or magnitude. Each included point is shaded based on their average outlier probability as determined by the MCMC. Many of those flagged as outliers may be non-members or members that do not follow the sequence (e.g., binaries). KOI-3876 is shown as a red star. The green lines are 200 PARSEC isochrones with parameters drawn (randomly) from the MCMC posterior.

We measured the equivalent width of the Li 6708 Å line for 22 stars (including KOI-3876) using the Coude spectra described in Section 3.1. Using our measured radial and rotation velocities from the BF analysis, we shifted each spectrum to zero velocity and compared it to a rotationally broadened template of the same $T_{\rm eff}$. We then interactively defined regions of continuum between 6685 and 6730 Å, and the bounds of the EW integration. We measured the Li EW and its uncertainty using a bootstrap approach. The continuum was first fit using `emcee`, 1000 random draws from the fit posterior are used to normalized the spectrum, and for each realization, the Li absorption line is numerically integration 10 times where the integration bounds are varied randomly from a normal distribution with the width of a resolution element. This procedure results in 10,000 Li EW measurements, we take the median and standard deviation as our final measurement and its uncertainty, respectively.

Past detections of Li with the same observational setup and our typical spectrum SNR indicate we were sensitive to Li down to equivalent widths of $20m\AA$ or better. So we report this as our upper limit when no line is detected. One star (Gaia EDR3 2052858307226740352) had a $v \sin i_* > 50$km s^{-1}, which made extraction of the Li line unreliable. So we instead reported a $< 70m\AA$ upper limit for this source based on past detections on similarly broadened spectra.

For KOI-3876, we estimated a Li equivalent width if $134\,m\AA$. This is marginally higher than (but consistent with) the value from Berger et al. (2018) ($120\,m\AA$). We attribute this difference to Berger et al. (2018)'s removal of the Fe line at 6707.44 Å. We did not attempt to correct for this contamination or from broad molecular contamination in the cooler stars. Fe line contamination likely set a limit on the precision of our equivalent widths at the $\simeq$10% level, comparable to the measurement errors. The difference was small compared to the offset in Li levels between clusters; we used our Li measurements for all targets for consistency.

Two spectra (Gaia EDR3 2101333021814076800 and 2048317736525727488) had two clear sets of lines, indicating an SB2. For our Li measurements, we measured each line individually with a manually-applied velocity offset. We then combined the two equivalent widths.

We compared the Li sequence for MELANGE-2 to that from the $\simeq$112 Myr Pleiades Bouvier et al. (2018) and the 650-700 Myr Hyades from (Cummings et al. 2017) in Figure 7. The MELANGE-2 sequence is nearly identical to that from Pleiades. The Li sequences of nearby clusters from `BAFFLES` (?) suggested an age between 85 Myr and 200 Myr, consistent with our isochronal age. This age range is conservative, as the bounds can only be set using the set of clusters with ages and extant lithium sequence measurements. For the upper bound, this was set by M34 and M35 (200-300 Myr).

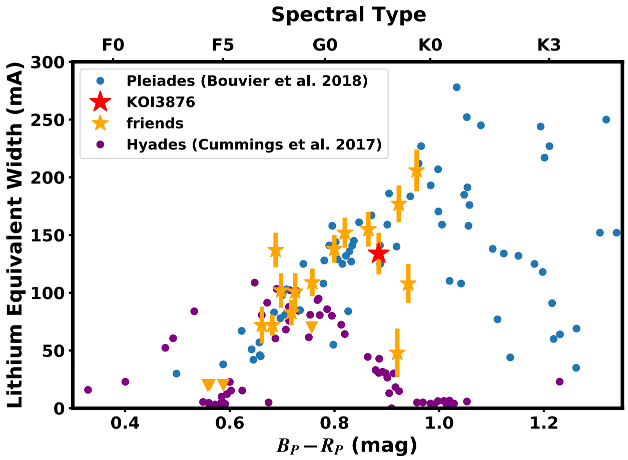

Figure 7. Lithium equivalent width as a function of *Gaia* $B_P - R_P$ color for candidate members of KOI-3876 (MELANGE-2; orange), KOI-3876 (red), and members of the 125 Myr Pleiades from Bouvier et al. (2018) and ≃700 Myr Hyades (Cummings et al. 2017). Triangles indicate upper limits. We have excluded MELANGE-2 candidates with velocities inconsistent with membership. The MELANGE-2 sequence is consistent with that from Pleiades members; only one star has an anomalously low Li (Gaia EDR3 2044150037698600448) compared to the Pleiades sequence. The high levels of Lithium seen in the mid-G dwarfs alone demonstrate that MELANGE-2 is much younger than Hyades.

5.4. *Rotation*

To better constrain the age of MELANGE-2 (and hence KOI-3876), we attempted to determine rotation periods for all candidate members using *Kepler* rotation measurements from the literature or our own measurements from *Kepler* data or *TESS* full-frame images (FFIs). The light curve extraction and literature search are described in Section 3.2.2.

For our own measurements, we searched the single-quarter *Kepler* or *TESS* light curves for rotation periods between $0.1 - 50$ days using the Lomb-Scargle algorithm (Horne & Baliunas 1986) for each quarter for each star with available *Kepler* data. We selected the initial rotation from the quarter returning the rotation period with the highest periodogram power. To confirm these measurements, we phase-folded the single-quarter light curves to the discovered period and examined the signals' consistency across quarters. We performed an eye-check in the style of Rampalli et al. (2021), labeling obvious rotations as Q0, questionable rotations as Q1, spurious detections as Q2, and non-detections as Q3. In total, 11 of the stars with *Kepler* data and no literature rotation returned usable rotations of quality Q0 or Q1.

For the rest of the candidates without rotations found in the literature or through our *Kepler* light curve measurements, we searched for signatures of rotation in CPM light curves extracted from the *TESS* Full Frame Image data (see Section 3.2). After searching each single-sector light curve of each star for rotation periods from $0.1 - 30$ days using the Lomb-Scargle algorithm, we repeated the same rotation selection and quality check procedure as outlined for the *Kepler* data. We found 64 quality Q0 or Q1 rotations from the *TESS* CPM-subtracted light curves available.

Based on variations in the extracted rotation period between *TESS* sectors and/or *Kepler* quarters, we estimate rotation period errors to be ≃10% for our own measurements. This larger than the expected errors just considering signal-to-noise and Lomb-Scargle errors from bootstrapping, likely due to differential rotation and spots appearing and disappearing on the surface of the star.

In total, we were able to assign rotation periods to 131 candidate members, all of which are reported in Table 4; 67 periods were determined based on *Kepler* data and 64 from *TESS*. The rotation period distribution (Figure 8) is extremely consistent with that from the Pleiades, further validating the age from our Li measurements and isochrone fit. Approximately 92 of these have rotation periods consistent with the Pleiades sequence. Most of the slower rotators are likely field interlopers, as they are (statistically) further from KOI-3876 in both three-dimensional distance and tangential velocity.

Of 1007 initial candidates, only having 92 stars with Pleiades-like rotation periods initially appears as a low success rate for a young association. However, the overwhelming majority of the other 876 stars were stars where no rotation period could be measured even if one is present (mostly due to intrinsic faintness). For example, of the 935 stars with a matching TIC ID, but no rotation period from *Kepler* data, 751 were either too faint ($T \gtrsim 15$) or too contaminated by nearby stars to extract a usable CPM curve. An unknown further set of stars had light curves but may have had rotation amplitudes below detectable levels due to poor SNR. Thus, the difference is mostly a measure of how *Gaia* can retrieve precise astrometry for stars far fainter than *Kepler* and *TESS* can provide rotation periods for.

Instead, we estimated the field contamination rate using just the stars where it is likely we would detect a rotation period. We selected the XXX stars with $0.4 < G - R_P < 0.8$, which approximately corresponds to FX to KY. Of these XXX stars, YYY have rotation periods consistent with Pleiades. This suggests about ZZ% of candidate members are true members.

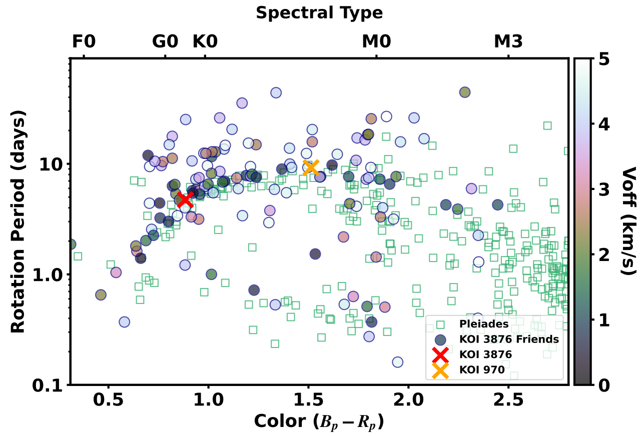

Figure 8. Rotation periods candidate members of MELANGE-2 (dark circles). Only literature measurements or stars with Q0 or Q1 rotations are shown. For reference, we show rotation periods from $\simeq$110 Myr Pleiades (green squares; cite Rebull 2016 Multiperiod Pleiades stars). Stars are color-coded by their tangential velocity difference compared to KOI-3876. Statistically, the stars on the Pleiades gyrochrone are also closer to KOI-3876 in tangential velocity. Because of the distance to the cluster, we have few rotation periods past M1.

6. PARAMETERS OF THE PLANET HOSTS KOI-3876 b

We summarize constraints on the host star in Table 2, the details of which we provide in in this section.

6.1. *Literature Parameters*

As a reasonably bright ($K_P = 12.6$) star hosting a planet candidate from the *Kepler* mission, KOI-3876 has numerous stellar parameters in the literature. The California *Kepler* Survey estimate $T_{\rm eff}$=5720 $\pm$ 60 K, *log g* =4.64$\pm$0.1, and $v \sin i_*$=9.9$\pm$1.0km s^{-1}, $R_*0.95^{+0.06}_{-0.04}R_\odot$ and $M_* = 1.01{\pm}0.03M_\odot$ based on comparing their high-resolution spectra and comparison to well-characterized templates (Petigura et al. 2017; Yee et al. 2017) and stellar isochrones (Johnson et al. 2017). Brewer & Fischer (2018), using the same spectra, estimate $T_{\rm eff}$=5642$\pm$27 K, *log g* =4.46$\pm$0.05, $R_* = 0.93{\pm}0.02M_\odot$, $M_* = 0.99 \pm 0.02M_\odot$, and $v \sin i_*$=10.4$\pm$0.5km s^{-1}, as well as detailed abundances that are generally consistent with the Solar value. Berger et al. (2020) incorporated *G*aia DR2 data with MIST stellar isochrones to derive an $T_{\rm eff}$=5577 $\pm$ 85 K, *log g* = 4.50 $\pm$ 0.02, and $R_* = 0.908 \pm 0.017R_\odot$.

These stellar parameters are generally in agreement with each other. However, those that relied on isochrones (Johnson et al. 2017; Brewer & Fischer 2018; Berger et al. 2020) assigned > 1 Gyr ages, much older than the true $\simeq$80 Myr age of KOI-3876. Although the assigned errors were large (and hence may be marginally consistent), the derived parameters may still be biased by the lack of an assigned age. Although this will not impact purely spectroscopic parameters like $T_{\rm eff}$ and $v \sin i_*$, the assumption can have a strong impact on the estimated stellar mass. Thus, we revisit these parameters with our own analysis below.

6.2. *Spectral-Energy Distribution*

.

We fit the observed spectral-energy-distribution (SED) following Mann et al. (2016a). To briefly summarize, we fit the observed photometry with a grid of optical and near-infrared flux-calibrated spectra spanning 0.4–2.3μm. We included BT-SETTL CIFIST atmospheric models (Baraffe et al. 2015) in the fit, both to estimate the $T_{\rm eff}$ and fill in gaps in the template spectra (e.g., beyond 2.3μm). We integrated the resulting absolutely-calibrated spectrum to estimate the bolometric flux ($F_{\rm bol}$), which we combined with the *G*aia EDR3 parallax to estimate the stellar luminosity (L_*). With $T_{\rm eff}$ and L_*, we calculated R_* using the Stefan-Boltzmann relation. While reddening in this sight-line is low (Schlafly & Finkbeiner 2011), KOI-3876 is well outside the Local Bubble, so we included extinction as part of the fit. To account for variability in the star, we added (in quadrature) 0.02 mags to the errors of all optical photometry. In total, the fit included six free parameters: the spectral template, A_V, three parameters that describe the model (log g, $T_{\rm eff}$, and [M/H]), and a scale factor between the model and the photometry. We show an example fit in Figure 9. The resulting fit yielded $A_V = 0.16^{+0.10}_{-0.08}$, $T_{\rm eff}$=5672 $\pm$ 65 K, $F_{\rm bol}$=(2.55 $\pm$ 0.10) $\times$ 10^{-10} (erg cm^{-2} s^{-1}), $L_* = 0.81 \pm 0.03L_\odot$, and $R_* = 0.94 = 0.03R_\odot$.

Our SED parameters were in good agreement with the literature spectroscopic values. Since the star is Sun-like, we considered the(high-resolution spectroscopic $T_{\rm eff}$ to be more reliable than the SED-based value, but the SED-based luminosity (and radius) more reliable than one derived from the spectroscopic *log g* or isochrone. We combined the two, which yielded a final radius of $0.92 \pm 0.02R_\odot$.

6.3. *Isochronal parameters*

To determine M_* and verify our other stellar parameters, we compared the observed photometry to Solar-metallicity magnetic DSEP evolution models and PARSEC models. We used `emcee` to simultaneously fit for age, A_V, M_*, and an additional parameter to capture underestimated uncertainties in the data or models (f, in magnitudes) within an MCMC framework. We used a

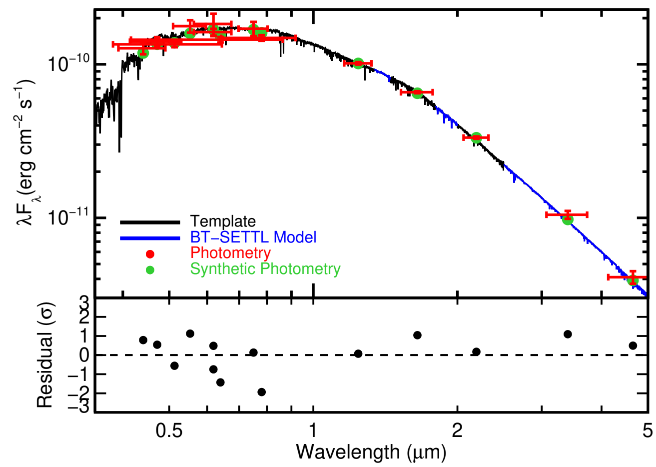

Figure 9. Best-fit template spectrum (G1V; black) and synthetic photometry (green) compared to the observed photometry of KOI-3876 (red). Errors on observed photometry are shown as vertical error bars, while horizontal error bars indicate the approximate width of the filter. BT-SETTL models (blue) were used to fill in regions of high telluric absorption or beyond the template range. The bottom panel shows the photometric residual in units of standard deviations.

hybrid interpolation method, first identifying the nearest age in then model grid and then performing a linear interpolation in mass to obtain stellar parameters and model photometry. Since this method could not interpolate between ages, we re-sampled the input grid using the `isochrones` package (Morton 2015a) to be more dense (0.1 Myr and $0.01 M_\odot$) than expected errors. To redden the model photometry, we used `synphot` (Lim 2020) and the extinction law from Cardelli et al. (1989). We placed a Gaussian prior on age of 110±11 Myr, while other parameters evolved under uniform priors. The resulting fit from each model grid was very precise, but differences between the two grids suggest larger systematic errors. Considering these, the resulting parameters were generally in agreement with our spectroscopic constraints ($R_* = 0.968 \pm 0.07$, $A_V = 0.27 \pm 0.10$, $T_{\rm eff}$=5710 ± 60) and provided a stellar mass estimate of $M_* = 1.04 \pm 0.03 M_\odot$. We combined this with our earlier radius estimate to get an estimate of the stellar density ($\rho_* = 1.30 \pm 0.10 \rho_o dot$).

6.4. *Stellar inclination*

To test whether the stellar spin and planetary orbit are consistent with alignment, we computed the stellar inclination (i_*) from the $v \sin i_*$, $P_{\rm rot}$, and R_* values estimated above. In is simplest form, this calculation is $V = 2\pi R_*/P_{\rm rot}$, but requires additional statistical corrections (see Morton & Winn 2014; Masuda & Winn 2020). Here we followed the methodology described in Masuda & Winn (2020). The resulting stellar inclination was $i_* > 71°$ at 95% confidence and $i_* > 80°$ at 68% confidence. This is consistent with alignment with KOI-3876 b's orbital inclination.

Table 2. Properties of the host star KOI-3876.

Parameter	Value	Source
Astrometry		
α	290.440629	*Gaia* EDR3
δ.	38.523572	*Gaia* EDR3
μ_α (mas yr^{-1})	-4.154±0.010	*Gaia* EDR3
μ_δ (mas yr^{-1})	2.269±0.011	*Gaia* EDR3
π (mas)	3.0565±0.0093	*Gaia* EDR3
Photometry		
G_{Gaia} (mag)	12.6054±0.0028	*Gaia* EDR3
BP_{Gaia} (mag)	12.9642±0.0033	*Gaia* EDR3
RP_{Gaia} (mag)	12.0798±0.0041	*Gaia* EDR3
B (mag)	13.375 ± 0.094	APASS
V (mag)	12.655 ± 0.122	APASS
g' (mag)	13.038 ± 0.033	APASS
r' (mag)	12.456 ± 0.092	APASS
i' (mag)	12.323 ± 0.062	APASS
J (mag)	11.456 ± 0.02	2MASS
H (mag)	11.152 ± 0.016	2MASS
K_S (mag)	11.107 ± 0.019	2MASS
$W1$ (mag)	11.06 ± 0.023	ALLWISE
$W2$ (mag)	11.09 ± 0.020	ALLWISE
$W3$ (mag)	10.91 ± 0.094	ALLWISE
Kinematics & Position		
RV$_{\rm Bary}$ (km s^{-1})	-26.79±0.01	Jönsson et al. (2020)
Physical Properties		
$P_{\rm rot}$ (days)	4.69 ± 0.04	(McQuillan et al. 2014)
$v \sin i_*$(km s^{-1})	10.4 ± 0.5	Brewer & Fischer (2018)
i_* (°)	> 80	This work
$F_{\rm bol}$ (erg cm^{-2} s^{-1})	$(2.55 \pm 0.10) \times 10^{-10}$	This work
$T_{\rm eff}$ (K)	5720 ± 60	This work, CKS
[Fe/H]	0.12 ± 0.02	Brewer & Fischer (2018)
M$_\star$ (M$_\odot$)	1.01 ± 0.03	This work
R$_\star$ (R$_\odot$)	0.92 ± 0.02	This work
L$_\star$ (L$_\odot$)	0.81 ± 0.03	This work
$\rho_\star$ ($\rho_\odot$)	1.30 ± 0.10	This work
Age (Myr)	110 ± 11	This work

7. PARAMETERS OF KOI-3876 b

We fit the *Kepler* photometry using the `misttborn` (MCMC Interface for Synthesis of Transits, Tomography, Binaries, and Others of a Relevant Nature) fitting code[3] first described in Mann et al. (2016b) and expanded upon in Johnson et al. (2018). `misttborn` uses `BATMAN` (Kreidberg 2015) to generate model light curves and `emcee` (Foreman-Mackey et al. 2013) to explore the transit parameter space.

[3] https://github.com/captain-exoplanet/misttborn

The standard implementation of `misttborn` fits for six parameters for each transiting planet: time of periastron (T_0), orbital period of the planet (P), planet-to-star radius ratio ($R_p/R_\star$), impact parameter (b), and stellar density ($\rho_\star$). For each wavelength observed, we fit two linear and quadratic limb-darkening coefficients (q_1, q_2) following the triangular sampling prescription of Kipping (2013). To cover all four bands (*TESS* and SDSS *griz*) required ten limb-darkening parameters in total. Gas drag and gravitational interactions are expected to dampen out eccentricities and inclinations of extremely young planets like KOI-3876 b (Tanaka & Ward 2004), so we locked the eccentricity at zero.

We ran two versions of the fit. In the first, the MCMC chain restricted e to 0 and allowed $\rho_\star$ to vary within a uniform distribution, and the second allowed e to vary with a Gaussian prior on $\rho_\star$ from our spectroscopic and SED analysis (Section 6). For both fits, applied Gaussian priors on the limb-darkening coefficients based on the values derived using our stellar parameters from Section 6 and the `LDTK` toolkit Parviainen & Aigrain (2015), with errors accounting for the difference between models (0.42±0.08 and 0.13±0.04 for linear and quadratic terms, respectively). All other parameters were sampled uniformly with physically motivated boundaries; e.g., T_0 was restricted to the time period sampled by the data and $|b| < 1 + R_P/R_*$.

To model stellar variations, `misttborn` includes a Gaussian Process (GP) regression module, utilizing the `celerite` code (Foreman-Mackey et al. 2017). We used a mixture of two stochastically driven damped simple harmonic oscillators (SHOs) at periods P_{GP} (primary) and $0.5P_{GP}$ (secondary). In total, there were five GP parameters: the log of the dominant period ($\ln(P_{GP})$), the log of the GP amplitude ($\ln$ Amp), a decay timescale for the variability (quality factor, $\ln Q0$), the difference between the primary and secondary quality factors ($\ln \Delta Q$), and a mix parameter that describes how the primary and secondary signals are combined (Mix). All GP parameters evolved under uniform priors.

We ran the MCMC using 50 walkers for 250000 steps including a burn-in of 20000 steps. The total run was more than 50 times the autocorrelation time (for both fits), indicating that the total run was sufficient for convergence.

As we show in Figures 10, the SHOs GP did an excellent job describing the overall variability, even in the presence of complex changes in the light curve morphology during the 4.5 years it was observed by *Kepler*. We also show the phase folded light curve in Figure 11 for the fit where e was allowed to vary. The best-fit parameters with uncertainties for both fits can be found in Table 3, and the corner plot for the major transit-fit parameters for the eccentric fit is in Figure 12.

The first fit ($e = 0$) yields a $\rho_\star$ value much larger than the spectroscopic/isochronal value determined in Section 6 ($15.5\rho_\odot$ vs $1.3\rho_\odot$). Although the error on the transit-fit density is large ($5.9\rho_\odot$), so the two values are consistent at $\simeq 2.5\sigma$. But this suggests the planet is likely to be eccentric. Indeed, in the fit where e is allowed to float, the preferred e is 0.2–0.4. For this reason, we adopt the second fit, where e is allowed to float, as the preferred fit.

7.1. *False Positive Analysis*

In Morton et al. (2016), the authors run the false-positive probability calculator `VESPA` Morton (2015b) on all *Kepler* objects of interest available at the time, which included KOI-3876 b. They assigned a high probability that KOI-3876 b (90%) that KOI-3876 b is an eclipsing binary, and < 1% that the signal is due to a planet overall. This conclusion was based primarily on the light curve morphology and available stellar parameters.

As we show in Figure 13, radial velocities from the Apache Point Observatory Galactic Evolution Experiment 16th data release (APOGEE DR16; Jönsson et al. 2020) rule out any stellar companion at the period of the planet. Further, our light curve analysis shows the expected U-shape transit for a planet, and there is no sign of a companion in the extant spectroscopy or adaptive optics imaging and non-redunant aperture masking from Kraus et al. (2016). *G*aia EDR3 astrometry and imaging similarly shows no sign of a companion. There is only one star detected with the *Kepler* PSF, which is too faint to reproduce the transit.

KOI-3876 also has a low Renormalised Unit Weight Error (RUWE) in EDR3 (0.94)

RUWE value is effectively an astrometric reduced χ^2 value, normalized to correct for color and brightness dependent effects[4]. RUWE should be around 1 for well-behaved sources, and higher values (RUWE$\gtrsim$1.3) suggests with the presence of a stellar companion (Ziegler et al. 2020; Wood et al. 2021).

It is possible the high Morton et al. (2016) was an artifact of poor detrending of the high stellar variability in KOI-3876 and/or the mismatch between the transit duration and that expected for a circular orbit (see Section 7). This motivated a

[4] https://gea.esac.esa.int/archive/documentation/GDR2/Gaia_archive/chap_datamodel/sec_dm_main_tables/ssec_dm_ruwe.html

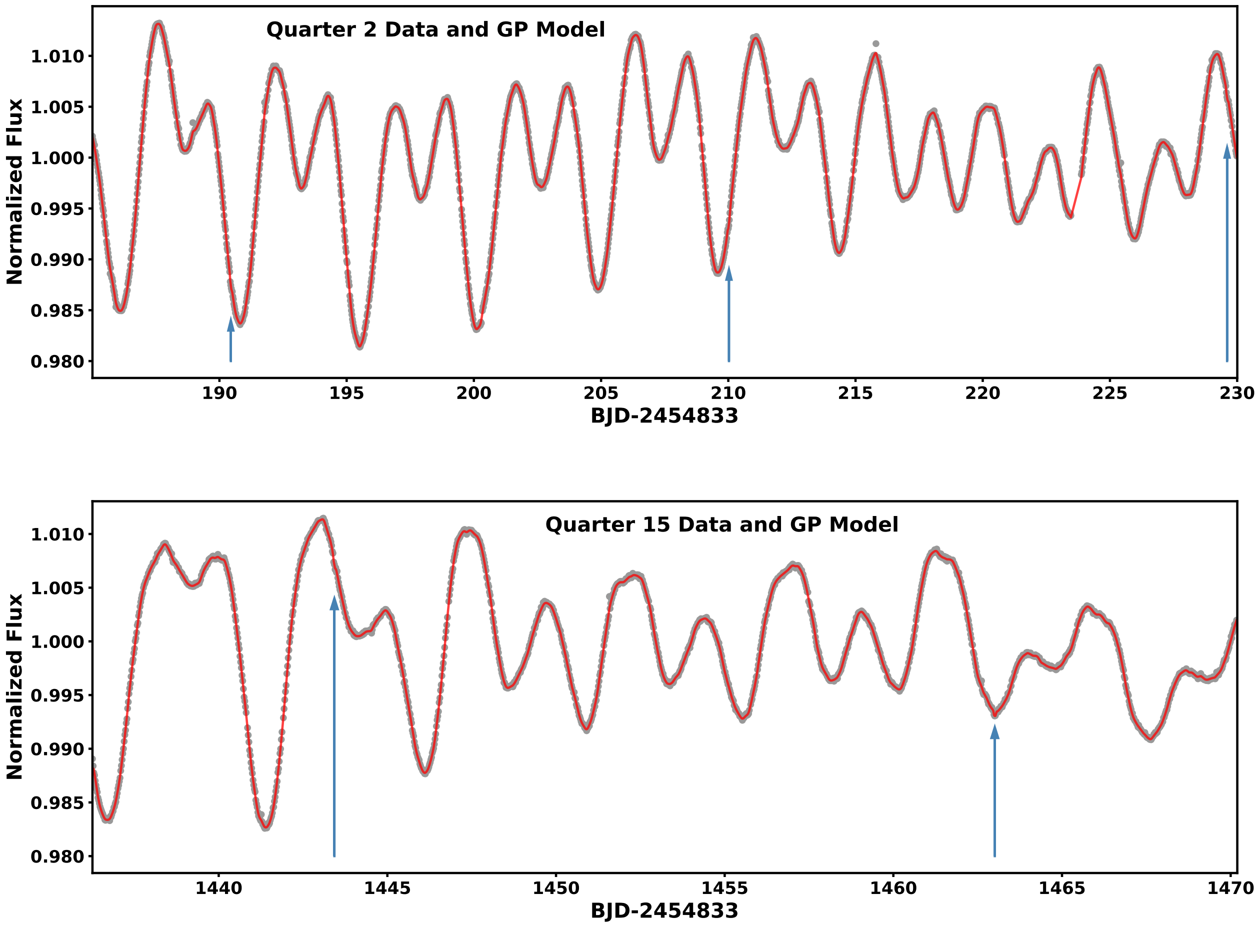

Figure 10. Approximately 40-day windows from *Kepler* Quarter 2 (top) and *Kepler* Quarter 15 (bottom) light curve of KOI-3876. The normalized flux (grey) is shown with our best-fit GP model (red). The locations of transits are shown with the blue arrows.

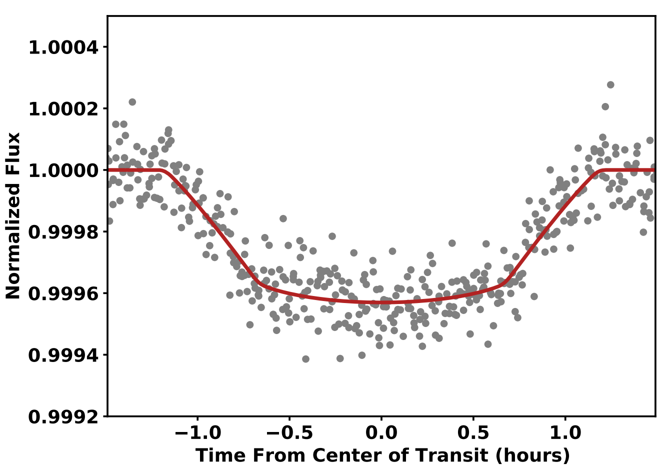

Figure 11. Phase-folded light curve of KOI-3876 from *Kepler* (grey points) with the best-fit transit model (red). The best-fit GP model to the stellar variability has been removed from both the data and the model for clarity. P

Rerunning the VESPA analysis, we find a 97% probability KOI-3876 b is a planet and a 3% probability KOI-3876 b is an eclipsing binary. As previously stated, shown in Figure 13, a stellar companion to KOI-3876 is ruled out at the period of the planet. Therefore, we conclude KOI-3876 b is a planet.

AWM: do we want to say something about the AO imaging somewhere.

8. SUMMARY AND CONCLUSIONS

KOI-3876 b is a $\simeq$ 110 Myr planet in the newly identified MELANGE-2 association. KOI-3876 b is about twice the size of the earth, orbiting a star that is a young analog to the Sun, having a similar radius and mass. Originally flagged as a false positive by //false positive work//, we rule out this disposition based on APOGEE radial velocities and our own light curve analysis. We see that the radial velocity dispersion of the system is not well-modeled by a stellar-mass body, ruling out the

Table 3. Parameters of KOI-3876

Parameter	Values	
	e=0	e float (preferred)
Measured Parameters		
T_0 (BJD-2454833)	131.71494 ± 0.00087	$131.71488^{+0.00089}_{-0.0009}$
P (days)	$19.577829 \pm 2.1 \times 10^{-5}$	$19.57783^{+2.2\times10^{-5}}_{-2.3\times10^{-5}}$
$R_P/R_\star$	$0.01946^{+0.00061}_{-0.00043}$	$0.02112^{+0.00092}_{-0.00079}$
b	$0.31^{+0.28}_{-0.22}$	$0.803^{+0.081}_{-0.1}$
$\rho_\star$ ($\rho_\odot$)	$15.5^{+2.5}_{-5.9}$	$1.308^{+0.09}_{-0.089}$
$q_{1,1}$	$0.291^{+0.107}_{-0.099}$	$0.305^{+0.101}_{-0.096}$
$q_{2,1}$	$0.371^{+0.075}_{-0.086}$	$0.373^{+0.077}_{-0.09}$
$\sqrt{e}\sin\omega$	–	$0.29^{+0.16}_{-0.22}$
$\sqrt{e}\cos\omega$	–	-0.07 ± 0.48
$\log(P_{GP})$	1.5658 ± 0.0036	$2.09^{+0.012}_{-0.5}$
$\log(Amp)$	$-9.48^{+0.13}_{-0.12}$	$-9.348^{+0.095}_{-0.2}$
$\log(\Delta Q)$	2.41 ± 0.22	$108.7^{+170.0}_{-110.0}$
$\log(Q0)$	$1.36^{+0.059}_{-0.056}$	$1.195^{+0.162}_{-0.08}$
$\log(Mix)$	$-1.56^{+0.16}_{-0.17}$	$3.6^{+4.2}_{-5.1}$
Derived Parameters		
$a/R_\star$	$76.2^{+3.9}_{-10.0}$	$40.2^{+4.1}_{-4.4}$
i (°)	$89.76^{+0.17}_{-0.29}$	$88.56^{+0.19}_{-0.13}$
T_{14} (days)	$0.0794^{+0.0016}_{-0.0015}$	$0.097^{+0.044}_{-0.019}$
T_{23} (days)	$0.0756^{+0.0015}_{-0.0016}$	$0.085^{+0.042}_{-0.02}$
a (AU)	$0.326^{+0.018}_{-0.049}$	0.165 ± 0.029
e	...	$0.27^{+0.16}_{-0.14}$
ω (°)	...	$114.0^{+55.0}_{-73.0}$

possibility of an eclipsing binary. The scatter in radial velocity is likely due to the stellar jitter that is common in young stars since the variation is still below expected for even a tight eclipsing binary.

We used rotation periods, lithium, and isochronal evolution models in order to age MELANGE-2 and thus KOI-3876 b to 110 ± 10 Myr. Based on //theia work//, we conclude that MELANGE-2may(not) be a subgroup of the larger Theia 316 association. //Theia 316 conclusion// Due to the high number of stars too faint for radial velocity and Lithium follow-up, it is uncertain whether or not these groups overlap.

Using misttborn, we find that KOI-3876 b likely has an eccentric orbit. We find that we can only match the fitted stellar density and the estimated isochronal density by allowing the eccentricity to vary in the fit rather than fixing it to 0. Because of this, we prefer the eccentric fit parameters over the fixed eccentricity fit.

Further, we identified additional candidates in the association for future follow-up that have potential of being planetary candidates. Due to the low SNR of the targets, we simply call these candidates in need of follow up.

The THYME collaboration would like to acknowledge Halee, who kept Madyson sane during lockdown.

MGB was supported by the NC Space Grant Undergraduate Research program and by funding from the Chancellor's Science Scholars Program at the University of North Carolina at Chapel Hill.

REFERENCES

Aigrain, S., Llama, J., Ceillier, T., et al. 2015, MNRAS, 450, 3211, doi: 10.1093/mnras/stv853

Anguiano, B., Majewski, S. R., Allende Prieto, C., et al. 2018, A&A, 620, A76, doi: 10.1051/0004-6361/201833387

Angus, R., Aigrain, S., Foreman-Mackey, D., & McQuillan, A. 2015, MNRAS, 450, 1787, doi: 10.1093/mnras/stv423

Baraffe, I., Homeier, D., Allard, F., & Chabrier, G. 2015, A&A, 577, A42, doi: 10.1051/0004-6361/201425481

Barnes, S. A. 2007, ApJ, 669, 1167, doi: 10.1086/519295

Berger, T. A., Howard, A. W., & Boesgaard, A. M. 2018, ApJ, 855, 115, doi: 10.3847/1538-4357/aab154

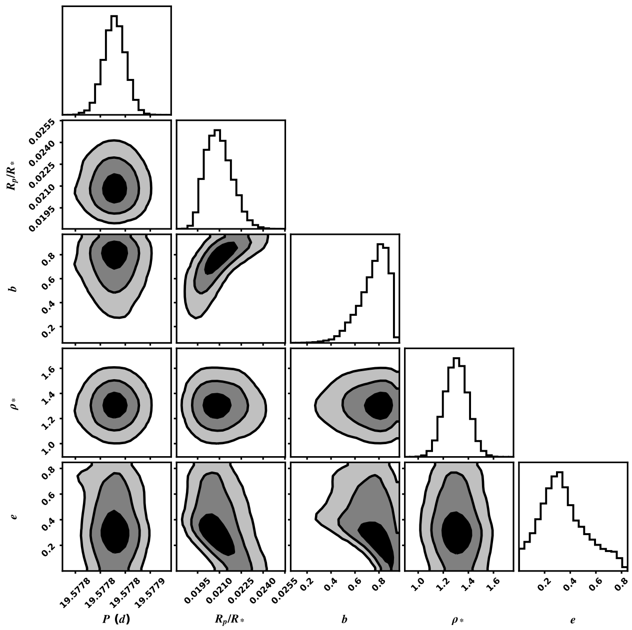

Figure 12. Corner plot of the major transit parameters (P, R_P/R_*, b, ρ_*, and e) from our `MISTTBORN` fit. The contour levels correspond to 1σ, 2σ, and 3σ of the points (from darkest to lightest). The planet-to-star radius ratio and eccentricity are strongly covariant with impact parameter, as a higher impact parameter requires a deeper transit (and lower eccentricity) to reproduce the observed transit depth (and duration). Plot made using corner.py (Foreman-Mackey 2016).

Berger, T. A., Huber, D., Gaidos, E., van Saders, J. L., & Weiss, L. M. 2020, AJ, 160, 108, doi: 10.3847/1538-3881/aba18a

Bouvier, J., Barrado, D., Moraux, E., et al. 2018, A&A, 613, A63, doi: 10.1051/0004-6361/201731881

Brems, S. S., Kürster, M., Trifonov, T., Reffert, S., & Quirrenbach, A. 2019, A&A, 632, A37, doi: 10.1051/0004-6361/201935520

Bressan, A., Marigo, P., Girardi, L., et al. 2012, MNRAS, 427, 127, doi: 10.1111/j.1365-2966.2012.21948.x

Brewer, J. M., & Fischer, D. A. 2018, ApJS, 237, 38, doi: 10.3847/1538-4365/aad501

Brown, T. M., Latham, D. W., Everett, M. E., & Esquerdo, G. A. 2011, AJ, 142, 112, doi: 10.1088/0004-6256/142/4/112

Cardelli, J. A., Clayton, G. C., & Mathis, J. S. 1989, ApJ, 345, 245, doi: 10.1086/167900

Corsaro, E., Stello, D., Huber, D., et al. 2012, ApJ, 757, 190, doi: 10.1088/0004-637X/757/2/190

Cummings, J. D., Deliyannis, C. P., Maderak, R. M., & Steinhauer, A. 2017, AJ, 153, 128, doi: 10.3847/1538-3881/aa5b86

Curtis, J. L., Agüeros, M. A., Douglas, S. T., & Meibom, S. 2019, ApJ, 879, 49, doi: 10.3847/1538-4357/ab2393

Cutri, R. M., & et al. 2014, VizieR Online Data Catalog, II/328

Dotter, A., Chaboyer, B., Jevremović, D., et al. 2008, ApJS, 178, 89, doi: 10.1086/589654

Feiden, G. A., & Chaboyer, B. 2012, ApJ, 761, 30, doi: 10.1088/0004-637X/761/1/30

Foreman-Mackey, D. 2016, The Journal of Open Source Software, 1

Foreman-Mackey, D., Agol, E., Ambikasaran, S., & Angus, R. 2017, AJ, 154, 220, doi: 10.3847/1538-3881/aa9332

Foreman-Mackey, D., Hogg, D. W., Lang, D., & Goodman, J. 2013, PASP, 125, 306, doi: 10.1086/670067

Gaia Collaboration, Prusti, T., de Bruijne, J. H. J., et al. 2016, A&A, 595, A1, doi: 10.1051/0004-6361/201629272

Gaia Collaboration, Brown, A. G. A., Vallenari, A., et al. 2021, A&A, 649, A1, doi: 10.1051/0004-6361/202039657

Gray, D. F. 1992, The observation and analysis of stellar photospheres., Vol. 10 (Camb. Astrophys. Ser)

Green, G. M., Schlafly, E., Zucker, C., Speagle, J. S., & Finkbeiner, D. 2019, ApJ, 887, 93, doi: 10.3847/1538-4357/ab5362

Hattori, S., Foreman-Mackey, D., Hogg, D. W., et al. 2021, arXiv e-prints, arXiv:2106.15063. https://arxiv.org/abs/2106.15063

Henden, A. A., Templeton, M., Terrell, D., et al. 2016, VizieR Online Data Catalog, II/336

Hogg, D. W., Bovy, J., & Lang, D. 2010, arXiv e-prints, arXiv:1008.4686. https://arxiv.org/abs/1008.4686

Horne, J. H., & Baliunas, S. L. 1986, ApJ, 302, 757, doi: 10.1086/164037

Husser, T.-O., Wende-von Berg, S., Dreizler, S., et al. 2013, A&A, 553, A6, doi: 10.1051/0004-6361/201219058

Johnson, J. A., Petigura, E. A., Fulton, B. J., et al. 2017, AJ, 154, 108, doi: 10.3847/1538-3881/aa80e7

Johnson, M. C., Dai, F., Justesen, A. B., et al. 2018, MNRAS, 481, 596, doi: 10.1093/mnras/sty2238

Jönsson, H., Holtzman, J. A., Allende Prieto, C., et al. 2020, AJ, 160, 120, doi: 10.3847/1538-3881/aba592

Katz, D., Sartoretti, P., Cropper, M., et al. 2019, A&A, 622, A205, doi: 10.1051/0004-6361/201833273

Kerr, R., Rizzuto, A. C., Kraus, A. L., & Offner, S. S. R. 2021, arXiv e-prints, arXiv:2105.09338. https://arxiv.org/abs/2105.09338

Kiman, R., Faherty, J. K., Cruz, K. L., et al. 2021, arXiv e-prints, arXiv:2104.01232. https://arxiv.org/abs/2104.01232

Kipping, D. M. 2013, MNRAS, 435, 2152, doi: 10.1093/mnras/stt1435

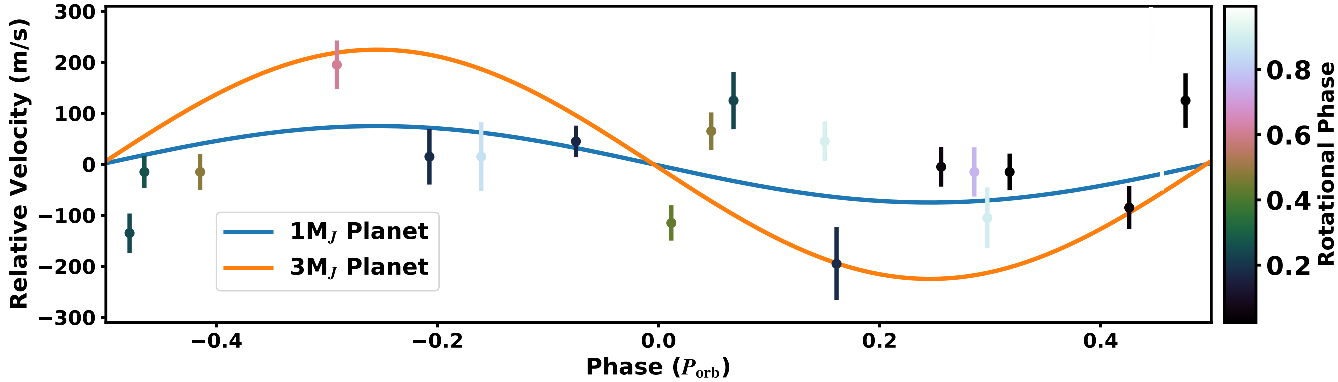

Figure 13. Radial velocities from APOGEE (Jönsson et al. 2020) for KOI-3876 as a function of the planet's orbital phase and colored by the rotational phase. The velocities rule out any companion more massive than $\simeq 2M_J$, ruling out any possibility of an eclipsing binary at the transit period. The scatter is larger than expected for the uncertainties by $\simeq$100m s^{-1}, but this is most likely due to stellar jitter common in young stars (Brems et al. 2019; Tran et al. 2021), and this is still far below the expected variation for a tight eclipsing binary.

Kraus, A. L., Ireland, M. J., Huber, D., Mann, A. W., & Dupuy, T. J. 2016, AJ, 152, 8, doi: 10.3847/0004-6256/152/1/8

Kreidberg, L. 2015, PASP, 127, 1161, doi: 10.1086/683602

Krumholz, M. R., McKee, C. F., & Bland-Hawthorn, J. 2019, ARA&A, 57, 227, doi: 10.1146/annurev-astro-091918-104430

Lim, P. L. 2020, synphot, 1.0.1, Zenodo, doi: 10.5281/zenodo.3971036

Luo, A. L., Zhao, Y. H., Zhao, G., & et al. 2019, VizieR Online Data Catalog, V/164

Luo, A. L., Zhao, Y.-H., Zhao, G., et al. 2015, Research in Astronomy and Astrophysics, 15, 1095, doi: 10.1088/1674-4527/15/8/002

Mann, A. W., Newton, E. R., Rizzuto, A. C., et al. 2016a, AJ, 152, 61, doi: 10.3847/0004-6256/152/3/61

Mann, A. W., Gaidos, E., Mace, G. N., et al. 2016b, ApJ, 818, 46, doi: 10.3847/0004-637X/818/1/46

Mann, A. W., Wood, M. L., Schmidt, S. P., et al. 2021, arXiv e-prints, arXiv:2110.09531. https://arxiv.org/abs/2110.09531

Masuda, K., & Winn, J. N. 2020, AJ, 159, 81, doi: 10.3847/1538-3881/ab65be

McQuillan, A., Aigrain, S., & Mazeh, T. 2013, MNRAS, 432, 1203, doi: 10.1093/mnras/stt536

McQuillan, A., Mazeh, T., & Aigrain, S. 2014, ApJS, 211, 24, doi: 10.1088/0067-0049/211/2/24

Meibom, S., Barnes, S. A., Latham, D. W., et al. 2011, ApJL, 733, L9, doi: 10.1088/2041-8205/733/1/L9

Meibom, S., Torres, G., Fressin, F., et al. 2013, Nature, 499, 55, doi: 10.1038/nature12279

Meingast, S., Alves, J., & Fürnkranz, V. 2019, A&A, 622, L13, doi: 10.1051/0004-6361/201834950

Miglio, A., Brogaard, K., Stello, D., et al. 2012, MNRAS, 419, 2077, doi: 10.1111/j.1365-2966.2011.19859.x

Morton, T. D. 2015a, isochrones: Stellar model grid package. http://ascl.net/1503.010

—. 2015b, VESPA: False positive probabilities calculator, Astrophysics Source Code Library. http://ascl.net/1503.011

Morton, T. D., Bryson, S. T., Coughlin, J. L., et al. 2016, ApJ, 822, 86, doi: 10.3847/0004-637X/822/2/86

Morton, T. D., & Winn, J. N. 2014, ApJ, 796, 47, doi: 10.1088/0004-637X/796/1/47

Nielsen, M. B., Gizon, L., Schunker, H., & Karoff, C. 2013, A&A, 557, L10, doi: 10.1051/0004-6361/201321912

Parviainen, H., & Aigrain, S. 2015, MNRAS, 453, 3821, doi: 10.1093/mnras/stv1857

Petigura, E. A., Howard, A. W., Marcy, G. W., et al. 2017, AJ, 154, 107, doi: 10.3847/1538-3881/aa80de

Rampalli, R., Agüeros, M. A., Curtis, J. L., et al. 2021, arXiv e-prints, arXiv:2106.13250. https://arxiv.org/abs/2106.13250

Rizzuto, A. C., Mann, A. W., Vanderburg, A., Kraus, A. L., & Covey, K. R. 2017, AJ, 154, 224, doi: 10.3847/1538-3881/aa9070

Santos, A. R. G., Breton, S. N., Mathur, S., & García, R. A. 2021, ApJS, 255, 17, doi: 10.3847/1538-4365/ac033f

Santos, A. R. G., García, R. A., Mathur, S., et al. 2019, ApJS, 244, 21, doi: 10.3847/1538-4365/ab3b56

Schlafly, E. F., & Finkbeiner, D. P. 2011, ApJ, 737, 103, doi: 10.1088/0004-637X/737/2/103

Skrutskie, M. F., Cutri, R. M., Stiening, R., et al. 2006, AJ, 131, 1163, doi: 10.1086/498708

Smith, J. C., Stumpe, M. C., Van Cleve, J. E., et al. 2012, PASP, 124, 1000, doi: 10.1086/667697

Stassun, K. G., Oelkers, R. J., Paegert, M., et al. 2019, AJ, 158, 138, doi: 10.3847/1538-3881/ab3467

Stumpe, M. C., Smith, J. C., Van Cleve, J. E., et al. 2012, PASP, 124, 985, doi: 10.1086/667698

Tanaka, H., & Ward, W. R. 2004, ApJ, 602, 388, doi: 10.1086/380992

Tofflemire, B. M., Mathieu, R. D., & Johns-Krull, C. M. 2019, AJ, 158, 245, doi: 10.3847/1538-3881/ab4f7d

Tofflemire, B. M., Rizzuto, A. C., Newton, E. R., et al. 2021, AJ, 161, 171, doi: 10.3847/1538-3881/abdf53

Tran, Q. H., Bowler, B. P., Cochran, W. D., et al. 2021, AJ, 161, 173, doi: 10.3847/1538-3881/abe041

Tull, R. G., MacQueen, P. J., Sneden, C., & Lambert, D. L. 1995, PASP, 107, 251, doi: 10.1086/133548

Twicken, J. D., Jenkins, J. M., Seader, S. E., et al. 2016, AJ, 152, 158, doi: 10.3847/0004-6256/152/6/158

Van Cleve, J. E., Howell, S. B., Smith, J. C., et al. 2016, PASP, 128, 075002, doi: 10.1088/1538-3873/128/965/075002

van Saders, J. L., Ceillier, T., Metcalfe, T. S., et al. 2016, Nature, 529, 181, doi: 10.1038/nature16168

Walkowicz, L. M., & Basri, G. S. 2013, MNRAS, 436, 1883, doi: 10.1093/mnras/stt1700

Wood, M. L., Mann, A. W., & Kraus, A. L. 2021, arXiv e-prints, arXiv:2106.09040. https://arxiv.org/abs/2106.09040

Yee, S. W., Petigura, E. A., & von Braun, K. 2017, ApJ, 836, 77, doi: 10.3847/1538-4357/836/1/77

Ziegler, C., Tokovinin, A., Briceño, C., et al. 2020, AJ, 159, 19, doi: 10.3847/1538-3881/ab55e9

Table 4.

Gaia EDR3	α	δ	Gmag	$V_{\rm off}$	Spectral	TESS	Kepler	π	σ_π	$P_{\rm rot}$	$\sigma_{P_{\rm rot}}$	$P_{\rm rot}$	Li	$\sigma_{\rm li}$	RV	$\sigma_{\rm RV}$	RV
	(J2016)	(J2016)	(mag)	(km/s)	Class			(mas)	(mas)	(days)	(days)	ref	($m\AA$)	($m\AA$)	(km/s)	(km/s)	ref
2052827207364859264	290.44063	38.52357	12.605	0.000	G7.3	Y	Y	3.057	0.009	4.69	0.044	2	134.0	18.0	-26.088	0.026	5
2052804323776522624	290.46921	38.20201	18.977	3.554	M3.9	N	N	3.036	0.172	...	...	...	...	...	...	...	...
2100939194794324608	289.80783	38.95042	10.829	0.478	F4.4	Y	N	3.024	0.012	...	...	...	<20	...	-27.027	0.184	5
2052954995531623040	291.28017	39.20070	14.355	4.348	K4.7	N	Y	3.055	0.016	13.849	0.386	1, 2, 3	...	...	...	...	...
2100967537279486336	290.14895	39.26079	18.451	3.806	M4.1	N	N	3.094	0.136	...	...	...	...	...	...	...	...
2051102868195719168	290.43983	37.73210	17.503	0.516	M3.2	N	N	3.019	0.069	...	...	...	...	...	...	...	...
2053037660761796096	290.86832	39.65124	17.902	0.605	M3.7	N	N	3.067	0.084	...	...	...	...	...	...	...	...
2052645379929910144	290.91118	38.33558	13.747	0.988	K2.8	N	Y	2.996	0.033	5.264	...	4	...	...	-34.923	3.954	6
2052559995978462208	291.61221	37.79730	11.75	3.744	F9.3	Y	Y	3.082	0.01	10.94	0.151	1	...	...	-16.07	0.95	7
2100996639982248320	289.86923	39.64549	19.678	2.692	M3.7	N	N	3.083	0.322	...	...	...	...	...	...	...	...
2099426507311747200	289.44803	38.58778	17.385	0.897	M3.1	N	N	3.114	0.07	...	...	...	...	...	...	...	...
2052684790548985728	291.78531	38.46727	14.077	0.641	K4.6	N	N	3.009	0.038	...	...	...	...	...	...	...	...
2052858307226740352	290.54042	38.81248	11.42	0.350	F9.4	N	Y	2.978	0.019	2.76	0.174	1, 2	<20	...	-25.113	0.159	5
2053046907832580992	291.12056	39.64699	16.939	0.389	M2.6	N	N	3.003	0.046	...	...	...	...	...	...	...	...
2099289446315734784	288.78892	37.90815	10.835	0.240	F4.3	Y	N	3.099	0.011	...	...	...	<20	...	-27.461	0.125	5
2053001690416510720	291.56724	39.60279	18.441	0.159	M4.5	N	N	3.104	0.122	...	...	...	...	...	...	...	...
2052887478644057472	289.93506	38.64045	14.636	0.506	K5.3	N	Y	3.145	0.018	1.529	0.303	1, 2, 3	...	...	-35.304	5.175	6
2052807794117101312	290.53790	38.25958	14.736	3.776	K5.4	N	Y	2.971	0.031	7.595	0.265	1, 2, 3	...	...	...	...	...
2052517145084325888	291.05028	37.29823	19.789	0.587	M4.1	N	N	3.002	0.33	...	...	...	...	...	...	...	...
2053028319213859072	290.64738	39.41039	20.044	2.510	M2.4	N	N	3.141	0.449	...	...	...	...	...	...	...	...
2053384286102387200	291.63783	39.87497	16.359	1.316	M2.7	N	N	3.008	0.037	...	...	...	...	...	...	...	...
2099371153774293888	288.14566	38.42085	13.864	0.791	K3.3	N	Y	3.018	0.025	7.556	0.174	1, 2, 3	...	...	-49.734	5.424	6
2053444896681432704	291.46297	40.21305	17.606	4.287	M3.8	N	N	3.093	0.076	...	...	...	...	...	...	...	...
2051172511083958400	289.48378	37.33728	20.024	1.298	M2.3	N	N	3.137	0.394	...	...	...	...	...	...	...	...
2053078450072688000	291.08713	40.21787	15.897	4.996	M0.3	Y	Y	3.112	0.03	...	...	...	...	...	...	...	...
2101290488760369920	288.83978	40.10791	16.391	4.143	M2.5	N	N	3.024	0.135	2.254	...	4	...	...	...	...	...
2101187134663932544	290.69156	40.59631	19.858	4.582	M3.3	N	N	3.084	0.312	...	...	...	...	...	...	...	...
2099510688671686656	288.69978	39.12272	18.18	2.451	M4.1	N	N	3.145	0.326	...	...	...	...	...	...	...	...
2051660453728442112	292.99289	37.59955	18.4	4.180	M3.7	N	N	3.031	0.111	...	...	...	...	...	...	...	...

[a] Friends are targets less than 50 pc away and a tangential velocity within 5km s^{-1} of KOI-3876.

[b] Key for rotation period references: 1 = (McQuillan et al. 2013, 2014), 2 = (Nielsen et al. 2013), 3 = Santos et al. (2021, 2019), 4 = This work

[c] Indicates if the target had a light curve in *TESS* or *Kepler* of sufficient quality for running the Notch transit-search pipeline.

[d] Key for radial velocity references: 5 = Coude, 6 = LAMOSTDR5 (Luo et al. 2019), 7 = Gaia DR2 (Katz et al. 2019), 8 = APOGEE DR16 (Jönsson et al. 2020)